Title

Microenergy acoustic pulses promotes muscle regeneration through in situ activation of muscle stem cells

Journal

Journal of Orthopaedic Research®, 40(7)

ISSN

0736-0266

Authors

Zhang, He
Kim, Hubert T
Feeley, Brian T
et al.

Publication Date

2022-07-01

DOI

10.1002/jor.25184

Peer reviewed

HHS Public Access

Author manuscript

J Orthop Res. Author manuscript; available in PMC 2023 July 01.

Published in final edited form as:

J Orthop Res. 2022 July ; 40(7): 1621–1631. doi:10.1002/jor.25184.

Microenergy Acoustic Pulses Promotes Muscle Regeneration Through In-situ Activation of Muscle Stem Cells

He Zhang, PhD[a,b,c],

Hubert T. Kim, MD&PhD[b,c],

Brian T. Feeley, MD[b,c],

Guiting Lin, MD&PhD[d],

Tom F. Lue, MD[d],

Mengyao Liu, BA[b,c],

Lia Banie, BS[d],

Xuhui Liu, MD[b,c,#]

[a]Department of Physical Education, Central South University, Hunan, China

[b]Department of Orthopaedic Surgery, San Francisco Veterans Affair Health Care System, San Francisco, CA, USA

[c]Department of Orthopaedic Surgery, University of California at San Francisco, San Francisco, CA, USA

[d]Knuppe Molecular Urology Laboratory, Department of Urology, School of Medicine, University of California at San Francisco, San Francisco, CA, USA

Abstract

Microenergy Acoustic Pulses (MAP) is a modified low-intensity extracorporeal shock wave therapy that currently used for treating musculoskeletal disorders. However, its function on muscle regeneration after ischemia-reperfusion injury (IRI) remains unknown. This study aimed to explore the effect of MAP on muscle injury after IRI and its underlying mechanisms. 10-week-old C57BL/6J mice underwent unilateral hindlimb IRI followed with or without MAP treatment. Wet weight of tibialis anterior muscles at both injury and contralateral sides were measured followed with histology analysis at 3wks after IRI. In in-vitro study, the myoblasts, endothelial cells and fibro-adipogenic progenitors (FAP) were treated with MAP. Cell proliferation and differentiation were assessed, and related gene expressions were measured by real-time PCR. Our results showed that MAP significantly increased the muscle weight and centrally nucleated regenerating muscle fiber size along with a trend in activating satellite cells. In vitro data indicated that MAP promoted myoblast proliferation and differentiation and endothelial cells migration. MAP also induced FAP brown/beige adipogenesis, a promyogenic phenotype of FAPs. Our findings demonstrate the

[#]Corresponding author: Xuhui Liu, MD, 1700 Owens Street, San Francisco, CA 94158, Tel: 415-575-0546, Fax: 415-750-2181, liu.xuhui@ucsf.edu.

Author Contributions Statement: HZ, HK, BTF, GL, TFL and XL designed the experiments; HZ, ML, LB and XL conducted the experiments; HZ, ML and XL collected and analyzed the data; HZ, HK, BTF, GL, TFL, ML, LB and XL wrote the manuscript.

beneficial function of MAP in promoting muscle regeneration after IR injury by inducing muscle stem cells proliferation and differentiation.

Keywords

Microenergy Acoustic Pulses; muscle regeneration; ischemia-reperfusion; myoblast; endothelial cells; fibro-adipogenic progenitors

Introduction

Ischemia reperfusion (IR) is a pathological condition characterized by an initial restriction of blood supply to an organ followed by subsequent restoration of perfusion.[1] It is commonly seen in muscle injuries with vascular damages. Ischemia results in a severe imbalance of metabolic supply and the followed restoration of blood flow and re-oxygenation can cause even worse tissue injury and profound inflammatory response.[2] IR injury leads to severe muscle necrosis resulting in chronic muscle atrophy, degeneration and loss of limb function in effected individuals.[3,4] Promoting muscle regeneration and resume limb function after muscle IR injury remains a challenge up to date.

The low intensity extracorporeal shock wave therapy (Li-ESWT) has been used for treating musculoskeletal disorders recently.[5] It is reported that Li-ESWT can promote myogenesis[6] and is effective in preventing type I diabetes-related muscle atrophy in rats[7]. Recently, an improved technology of Li-ESWT named microenergy acoustic pulses (MAP) has been developed.[8,9] Compared to the traditional Li-ESWT and other shock wave-based therapies, the beam of the acoustic pulses of MAP is defocused to allow more even energy distribution to the treated tissue and eliminates the potential damage to issue at focal point.[10] We discovered that MAP ameliorated stress urinary incontinence (SUI) by enhancing regeneration of striated muscles in the external urinary sphincter and pelvic floor in rats.[9] Currently, MAP is under Phase III clinical trial for treating stress urinary incontinence (SUI) and expected to receive FDA approval for clinical use soon.

The goal of this study is to test the effect of MAP in improving muscle regeneration in the IR-induced muscle injury in a mouse model. We also sought to test the effect of MAP on myoblast, endothelial cell and fibro-adipogenic progenitor (FAP) cell proliferation and differentiation in order to understand the cellular mechanism of MAP-induced muscle regeneration. We hypothesize that MAP promotes muscle regeneration after IR injury.

Materials and Methods

Animals and procedures

Experiments were performed on 10-week-old male C57BL/6J mice (JAX, Cat# 000664). The mice were randomly divided into Control group and MAP group (n=6 in each group). Mice in both groups underwent unilateral hindlimb ischemia with a rubber band on the base of right thigh for 3 hours as previously described.[11] The other hindlimb was used as Contralateral side. The application of MAP treatment was performed on the same hindlimb at 1 week after the initial injury by using a compact electromagnetic unit with

an unfocused acoustic pulse source (LiteMed Inc, Taipei, Taiwan).[9] Animals were under general anesthesia and the shockwave probe was applied directly to the shaved tibialis anterior (TA) muscles and was coupled to the skin using ultrasound gel (Aquasonic, Parker Laboratories Inc, Fairfield, NJ). The MAP had an energy flux density at 0.059mJ/mm^2, and 500 pulses were delivered at 3Hz.[8] Mice in MAP group received treatment twice a week for 2 weeks.[12] Mice in the Control group received the sham procedure (including anesthesia) but no MAP treatment was applied. All the mice were housed in a neutral temperature environment on a 12/12h light/dark cycle and were provided with standard laboratory food and water. All experiments were approved by the Institutional Animal Care and Use Committee of our University.

Muscle harvesting and histology

After 2-weeks MAP treatment (3 weeks after initial IRI), all mice were sacrificed. TA muscles of both injury and contralateral sides from Control and MAP group (n=6 in each group) were harvested, weighed followed with histology analysis. Muscle samples were flash frozen by immersion in liquid nitrogen cool isopentane and sectioned at the thickness of 7 μm using cryostat. For immunofluorescence staining, slides were fixed in 4% paraformaldehyde and rinsed in PBS, incubated in blocking solution (0.1% Triton X-100, 2% bovine serum albumin in PBS) for 30 minutes at room temperature and then primary antibody solution (mouse anti-Pax7, DSHB, 1:50 and rabbit anti-Laminin, Sigma L9393, 1:200) at 4°C overnight. Slides were washed with PBS and treated with secondary antibody (donkey anti-mouse IgG Alexa Fluor® 647, Abcam, ab150107 and donkey anti-rabbit IgG Alexa Fluor® 488, Abcam, ab150073) at the concentration of 1:200. Tissue sections were stained with DAPI and then mounted with Fluoromount G. The M.O.M.™ kit (Vectorlabs, BMK-2202) was used for Pax7 stainning to avoid unspecific binding. The slides were reviewed by two blinded reviewers and cross-sectional area (CSA) was measured from at least 3 randomly chosen locations in the muscle belly for each sample with at least 40 fibers being counted in each location. Regenerating muscle was measured with central nucleation fiber rate (number of fibers with central nuclei / total fiber numbers × 100%). To evaluate the percentage of total Pax7$^+$ staining and Pax7$^+$ centralized nuclei, the total and Pax7$^+$ centralized nuclei numbers were divided by total DAPI × 100%. To evaluated vascularity in muscle (CD31 positive cells / total fiber numbers ×100%.), the slides were stained with CD31. Slides were fixed in cold acetone for 10 minutes and rinsed in PBS. After blocked in blocking solution (5% bovine serum albumin in PBS), the slides were incubated in primary antibody (rat anti-CD31, BioLegend B235098, 1:100) overnight at 4°C and then incubated with secondary antibody solution (goat anti-Rat IgG Alexa Fluor® 594, Abcam, ab150160, 1:200). The central nucleation fiber rate, total Pax7$^+$ / Pax7$^+$ centralized nuclei pervcentage and vascularity were measured from at least 3 different locations in the muscle belly for each samples.

Cell culture

Myoblast C2C12 cells were purchased from ATCC (ATCC® CRL-1772™). C2C12 were cultured in 12-well plates with 10% fetal bovine serum (FBS) in DMEM and then divided into Control and MAP group with 6 wells in each group. Before MAP treatment, removed the culture medium in the plate and the ultrasound gel were applied at the bottom of cell

plate. Placed the each well in MAP group on the shockwave probe and slightly moved the plate while being treated. All the MAP treatment was conducted at 0.033mJ/mm^2, 1Hz for 50 pulses.[13] To access the effect of MAP on cell proliferation, 24hrs after the cells treated with MAP, the Edu assay (Click-iT™ EdU Cell Proliferation Kit, ThermoFisher, C10337) was performed to determine the cell proliferation. To test the role of MAP in C2C12 myogenesis, the medium was changed to induction medium (2% horse serum in DMEM). When cells reached 80–90% confluent to induce myotube differentiation. The cells were then treated with MAP twice a week for 1 week. MHC (mouse anti-MF 20, DSHB, 1:100) staining was performed to determine the myoblast fusion index (the percentage of nuclei located in myotubes and all nuclei) and real-time PCR (RT-PCR) was conducted to measure gene expression that related to myogenesis.

Endothelial cell Endothelial cells were purchased from ATCC (ATCC® CRL-2581™) and cultured in Endothelial cell growth media (R&D system, CCM027). The cells were divided into Control and MAP group with 6 wells in each group Similarly, the Edu assay were performed 24hrs after the MAP treatment. The migration assay was applied to access the cell proliferation as well. Cells treated with MAP twice a week for 1 week before collected for RT-PCR.

Fibro-adipogenic progenitor (FAP) cell Primary FAP were isolated from muscle in C57BL/6J mice by flow cytometry as CD45$^-$/CD31$^-$/ Integrinα7$^-$/Sca1$^+$/CD140a$^+$.[14] FAPs were cultured in standard medium (10% FBS and 100ng/mL bFGF in F-10) and then divided into Control and MAP group with 5 wells in each group. Cells in MAP group were treated with MAP twice a week for 1 week. Cells were collected for immunofluorescent staining for adipogenesis (Perilipin, Sigma P1998) and fibrogenesis (α-SMA, Sigma SAB2500963) markers. For adipocyte differentiation, the medium was changed to adipogenesis induction medium (Gibco, A1007001) to induce cell differentiating into adipocytes. The adipocyte-differentiated cells were then treated with MAP twice a week for 1week and harvested for RT-PCR.

Edu assay

The Edu assay was conducted following the instructions. Briefly, the cells were incubated in10μM Edu working solution overnight at 37°C immediately after the MAP treatment. Cells were washed with PBS and then fixed with ice cold methanol for 10 minutes. After washed with PBST (0.1% Triton X-100 in PBS), cells were incubated in reaction cocktails containing 1X reaction buffer, $CuSO_4$, Alexa Fluor® azide and reaction buffer additive solution for 30 minutes at room temperature. Cells were washed and stained with DAPI.

Migration assay

The cell migration assay was performed as previously described.[15] Cells were plated in a 12-well plate for 100% confluent in 24hrs and a 200μl pipette tip was used to press firmly against the top of the tissue culture plate to make a vertical wound down through the cell monolayer. Following the generation and inspection of the wound an initial image was taken. Cell were cultured in serum free medium after MAP treatment. The wound closure images were taken at 8hr and 24hr time point. The wound area was measured using ImageJ

and a scatter plot was used to display the wound area over time. The wound closure rate was calculated according to the following formula: $V_{migration} = |slope| / 2 \times l$.[16] The *slope* was analyzed via Excel's Linear Trendline feature and l was the length of the wound. $V_{migration}$ was be expressed in units of μm/hour.

Real-time PCR

Cell RNA extraction and real-time PCR were conducted as previously reported.[17] Primer sequences of the genes tested are summarized in Table 1. The expression level of each gene was normalized to that of the housekeeping gene of 18s rRNA. Fold difference relative to controls was calculated using double delta cycle threshold. Three biological replicates were performed, and each real-time PCR reaction was run with three technical replicates to calculate expression.

Statistical analysis

The homogeneity test of variance was applied and the statistical difference between two groups was determined by Independent T-test or Welch's t-test. The statistical difference between multiple groups for cross sectional area, central nucleation, Pax7 and CD31 positive cell percentage was determined by Two-way ANOVA followed by Tukey *post doc* analysis. All data were analyzed with GraphPad Prism 8 and shown as mean ± SD. Statistical difference was determined when $P < 0.05$.

Results

MAP improves muscle regeneration with trend in activating satellite cell

T-test analysis showed that compared with the injured hindlimbs in Control group, the wet weight/body weight ratio of TA muscles from injured hindlimbs in MAP group significantly increased at 3-week time point after IR injury (2.870±0.597 vs 1.896±0.523 in Control, P=0.0132, n=6 in each group) (data not shown).

2-way ANOVA analysis showed a significant effect in IR injury (P=0.0004), but no significant effect was found in MAP (P=0.1141) and the interaction (P=0.7743) on cross sectional area.

After post-doc analysis, no significant change was found in average muscle CSA between MAP-IRI and Control-IRI group (1587.541±352.390 in MAP-IRI vs 1299.446±118.366 in Control-IRI, P=0.5293, n=6 in each group) (Figure 1A, B). However, the CSA of centrally nucleated fibers significantly increased with MAP treatment compared to injured muscles without any treatment 3 weeks after IRI analyzed by T-test (1769.475±218.071 vs 1542.188±115.468 in Control-IRI, P=0.0477, n=6 in each group) (Figure 1A, C). CSA distribution showed higher percentages of larger myofibers in injured hindlimbs treated with MAP compared to the Control group with no MAP treatment (Figure 1D).

Same with muscle cross sectional area, 2-way ANOVA analysis also indicated a significant effect in IR injury (P<0.0001) with no significant effect in MAP (P=0.9203) and the interaction (P=0.8996) on central nucleation. Muscle central nucleation in injured side significantly increased in both Control (86.136%±13.045% vs 0.617%±1.014%, P<0.01) and

MAP group (85.493%±4.146% vs 0.691%±0.904%, $P<0.01$) compared to its contralateral side analyzed by post-doc analysis, though no significant difference was seen in injured muscles between MAP and Control groups (85.493%±4.146% in MAP-IRI vs 86.136% ±13.045% in Control-IRI, $P=0.998$, n=6 in each group) (Figure 1A, E).

In terms of total $Pax7^+$ cell / DAPI percentage, 2-way ANOVA analysis only displayed a significant effect in IR injury ($P<0.0001$). No change was found in $Pax7^+$ cell / DAPI percentage between Control-IRI and MAP-IRI groups as well (17.196%±2.876 vs 16.607% ±2.145% in Control-IRI, $P=0.9923$, n=6 in each group) (Figure 1A, F) following post-doc analysis, but using T-test analysis, MAP showed a trend in increasing the $Pax7^+$ centralized nuclei when compared only injured muslces in both groups (10.319%±1.538 in MAP-IRI vs 8.407%±1.490% in Control-IRI, $P=0.0536$, n=6 in each group) (Figure 1A, G).

MAP significantly induces $CD31^+$ endothelial cell density after IR injury

Based on 2-way ANOVA analysis, the effects of IR injury and MAP treatment were both significant (IR injury: $P<0.0001$; MAP: $P=0.0002$), but the interaction of these two factors was considered not quite significant ($P=0.0842$). Following a post-doc analysis, the $CD31^+$ endothelial cell / total myofiber number percentage in the injured muscles was significantly higher than its contralateral side in Sham Control group (178.76%±19.80% vs 138.58% ±15.28% in Control-contralateral, $P=0.0083$, n=6 in each group) and in MAP treatment group (227.96%±21.72% vs 160.19%±18.31% in MAP-contralateral, $P<0.001$, n=6 in each group) three weeks after the initial IR injury. Mice treated with MAP showed an increased $CD31^+$ endothelial cell / total myofiber number percentage when compared the injured sides between MAP and its control group (227.96%±21.72% in MAP-IRI vs 178.76%±19.80% in Control-IRI, $P=0.001$, n=6 in each group), suggesting MAP increased $CD31^+$ endothelial cell density in regenerating muscles after IRI (Figure 2).

MAP promotes the proliferation and myogenesis of myoblast

T-test analysis showed that the Edu positive cell / DAPI percentage significantly increased after MAP treatment compared to its control group at 3-week (26.091%±3.168% vs 22.412%±4.152% in Control, $P<0.01$) (Figure 3A). MAP also significantly induced the fusion index in myoblast compared to the control group (19.267%±8.914% vs 14.942% ±6.792% in Control, $P=0.0122$) (Figure 3B). The expression levels of some myogenesis-related genes were significantly higher in MAP treated group compared to the control group as well (Myogenin: 3.248±1.543, $P=0.037$; MRF4: 2.382±0.447, $P<0.01$).

MAP promotes the proliferation and migration of endothelial cells

MAP treatment significantly induced the Edu positive cells compared to its control group using T-test analysis (16.99%±4.23% vs 14.72%±5.97% in Control, $P=0.0402$) (Figure 4A). Cell migration assay results showed that the wound area became smaller over time in both groups (Figure 4B, C). No significant change was found in wound area difference at 8hr (normalized wound area at 8hr to 0hr) between groups (65103.026±35405.118 vs 50846.215±24977.331 in Control, $P=0.1608$). However, the wound area difference at 24hr (normalized wound area at 24hr to 0hr) significantly increased in MAP-treated cells compared to cells in control group (324153.068±88853.670 vs 239993.642±68030.573 in

Control, P=0.0023) (Figure 4D). We calculated that the wound closure rate in control group was 66.92 μm/h and 90.39 μm/h in MAP group. Cells from MAP group displayed significantly higher mRNA expression in Fst-288 that involved in cell growth (fold change: 1.563±0.077, P=0.0014). IGF-1, Fst-315 had fold change increase of 1.321±0.147, 1.17±0.199 in that order, but no significant change was found (P>0.05) (Figure 4E).

MAP induces FAP beige/brown fat differentiation

T-test analysis showed that cells treated with MAP showed significantly higher UCP-1 expression which is a hallmark of beige/brown-like adipocytes (1.700%±0.406% vs 1.356% ±0.245% in Control, P=0.009) (Figure 5A). However, as the adipogenesis marker, no significant change was found in the Perilipin positive cell / DAPI percentage after MAP treatment (4.259%±1.857% vs 4.183%±1.707% in Control, P=0.8933) (Figure 5B, C), and MAP also displayed no effect on the fibrogenesis marker α-SMA (2.47%±0.718% vs 2.348%±1.138% in Control, P=0.658) (Figure 5 B, D). RT-PCR data showed a significant fold increase in expression of UCP-1 and PRDM16 in cells that cultured in adipogenesis medium from MAP group compared to control group (UCP-1: 3.027±0.357, P<0.01; PRDM16: 2.234±1.619, P=0.046). In addition, the growth factor genes IGF-1, Fst-315 and Fst-288 had significant fold increase of 5.592±4.031, 6.789±2.995 and 4.906±2.451, respectively (P<0.01) (Figure 5E).

Discussion

The extracorporeal shock wave therapy has been successfully used in treating multiple disorders, including achilles and knee tendinopathy,[18,19] diabetic nephropathy,[20] erectile dysfunction[21] and ischemic heart disease[22]. It has also been used as an alternative to surgery to treat recalcitrant painful heel syndrome, allowing fast recovery time without the necessity of reduced immobilization.[23] The shockwave of this therapy is usually quite well tolerated. Generally, no anesthesia or analgesics is needed since the discomfort during impulse application is mild. The safety profile of extracorporeal shock wave is well accepted by the field of physical therapies. The shock wave treatment can also be combined with other therapies to promote its efficacy. Several studies suggested that a combination of extracorporeal shock wave therapy and eccentric exercises was an effective treatment for insertional achilles tendinopathy.[24,25] MAP, a modified shock wave therapy with superior safety profile, showed an effect in inducing myogenesis of muscle stem cells and promoting muscle regeneration in vitro.[14,26] In this study, we further demonstrated the role of MAP in promoting muscle vascularity and contributing to improve muscle regerneration after IRI. Considering its excellent safety profile, MAP may serve as a potential therapy in patients to treat muscle injury in the future.

In this study, we observed a significant increase in muscle weight with the cross sectional area of the centrally nucleated fibers after MAP treatment, indicating that MAP may promote muscle regeneration after IRI. Muscle mounts a regenerative response upon injury which involves activating resident immune, satellite and interstitial cells that coordinate the clearance of cellular debris and generation of new fibers.[27] Satellite cell are the major cellular source contributing to myofiber repair.[28] They are predominately quiescent in the

mature resting muscles and will be activated to re-enter the cell cycle for muscle repair following muscle injury.[29] In this study, though we didn't see difference in the total $Pax7^+$ satellite cell percentage, we observed a trend of increasing $Pax7^+$ centralized nuclei in myofibers in MAP-treated group compared to the control group, suggesting MAP has a role in activating satellites cells myogenesis which may facilitate muscle regeneration after IRI. Centrally localized nuclei are hallmark of regenerating fibers, which is usually seen at the early stage of muscle regeneration.[30] A previous study has reported that increased number of central nucleated myofibers are observed early as 7 days after cardiotoxin (CTX)-induced muscle injury and this phenomenon lasts at least 14 days after injury.[31] This may partly explain that why we didn't see any significant change in central nucleation at the 3-week time point after the initial injury. In vitro data demonstrates that MAP promoted the myoblast myogenesis with an increase in gene expression of some key myogenic regulatory factors such as myogenin and MRF4 in C2C12 myoblasts. Taking together, results from current study provide the evidence of the role of MAP on myogenic stem cell activation during muscle regeneration after IR injury.

Vascularity is an important factor in muscle regeneration. Results from our study shows that MAP significantly increased proliferation and migration of endothelial cells that leads to the upregulation of the vascular density in muscle after IRI. The effect of extracorporeal shock wave therapy on microcirculation and blood vessel development has also been reported in previous human studies.[32,33] As one of the important stem/progenitor cells in muscle, endothelial cells have been found to support the muscle regenerating process. Besides providing blood supply, it can also secrete growth factors such as IGF-1 that influencing the proliferation and differentiation of satellite cells.[34] Follistatin (Fst), the activin-binding protein which enhances muscle growth[35] is found to express in endothelial cells as well[36]. In this study, we found that though MAP significantly increased the expression of Fst-288, the tissue isoform of follistatin in endothelial cell, it has no effect on expression of IGF-1 and Fst-315, the circulating isoform of follistatin. These data suggests that though MAP significantly increased vascular density in regenerating muscle, endothelia cell secreted growth factors may not be a mechanism of MAP induced muscle regeneration.

Another important progenitor cell population in muscle is the FAPs. These cells are believed to be the cellular source of fatty and fibrotic tissue accumulation in skeletal muscle in degenerative muscle diseases.[37] However, FAPs also play an important role in improving the performance of satellite cells and facilitating satellite cell myogenesis.[38] FAPs represent a source of pro-differentiation factors for driving myoblast fusion and differentiation .[39] Our in vitro results show that though MAP had no effect on reducing FAP adipogenesis and fibrogenesis, it significantly induced the expression of the uncoupling protein (UCP-1). UCP-1 is known as the hallmark of brown/beige fat whose differentiation is adopted by FAP cells,[40] implying MAP could stimulate the brown/beige fat differentiation of FAP cells. Besides its metabolic role in body, brown/beige fat can secrete several growth factors that promoting muscle growth.[37,41] Recently we found that brown/beige adipose tissue plays an important role in promoting muscle regeneration after rotator cuff injury.[42] Transplantation of beige FAPs significantly reduced muscle degeneration and improved shoulder function after massive cuff tears.[43] Our in vitro study further showed that MAP significant increased IGF-1 and Follistatin gene expression in FAPs. This suggests that inducing FAP brown/

beige differentiation may be one of the underlying mechanisms of MAP-mediated muscle regeneration.

There are some limitations of this study. First, only one time point was adopted in this study. In our previous and current studies, we find that robust muscle regeneration happens between 2 and 4 weeks after IRI.[44] Though a complete time course of muscle regeneration is favorable, we believe 3 weeks after IRI is an appropriate time point to evaluate the role of MAP on muscle injury. Second, no limb or muscle function was tested in this study. Though only histological results are included in current study, the “gold standard” is warranted to test function recovery after MAP treatment in future work. Third, only male C57B/L6 mice were used in this study. Future study is needed to address potential gender and strain difference in responding to MAP treatment after muscle IRI. Last but not least, we only selected one energy level of MAP which is based on studies focusing on other disorders in this experiment. More work is needed to test different MAP energy levels to investigate the optimal treatment protocol for IR injury in mouse model.

In conclusion, this study demonstrates the beneficial role of MAP in promoting muscle regeneration in ischemia reperfusion-induce injury through inducing muscle stem cells proliferation and differentiation. MAP could serve as a new treatment option in improving muscle regeneration in the near future.

Supplementary Material

Refer to Web version on PubMed Central for supplementary material.

Acknowledgments

This work was supported by NIH/NIAMS Research Grant (1R01AR072669-01A1, PI: Feeley), U.S. Department of Veterans Affairs, Veterans Health Administration, Office of Research and Development, Biomedical Laboratory Research and Development Merit Review Grant (1I01BX002680, PI: Kim) and R01 Grant (1R01DK124609, PI: Lue).

Reference

1. Eltzschig HK, Eckle T. 2011. Ischemia and reperfusion--from mechanism to translation. Nat Med 17(11):1391–401. [PubMed: 22064429]
2. Yellon DM, Hausenloy DJ. 2007. Myocardial reperfusion injury. N Engl J Med 357:1121–1135. [PubMed: 17855673]
3. Orfany A, Arriola CG, Doulamis IP, et al. 2020. Mitochondrial transplantation ameliorates acute limb ischemia. J Vasc Surg 71(3):1014–1026. [PubMed: 31353269]
4. Simon F, Oberhuber A, Floros N, et al. 2018. Acute Limb Ischemia-Much More Than Just a Lack of Oxygen. Int J Mol Sci 19(2):374.
5. Zissler A, Steinbacher P, Zimmermann R, et al. 2017. Extracorporeal Shock Wave Therapy Accelerates Regeneration After Acute Skeletal Muscle Injury. Am J Sports Med 45(3):676–684. [PubMed: 27729321]
6. Wang B, Zhou J, Banie L, et al. 2018. Low-intensity extracorporeal shock wave therapy promotes myogenesis through PERK/ATF4 pathway. Neurourol Urodyn 37(2):699–707. [PubMed: 28763567]
7. Tang L, Li N, Jian W, et al. 2017. Low-intensity pulsed ultrasound prevents muscle atrophy induced by type 1 diabetes in rats. Skelet Muscle 7(1):29. [PubMed: 29273088]

8. Kang N, Peng D, Wang B, et al. 2019. The effects of microenergy acoustic pulses on animal model of obesity-associated stress urinary incontinence. Part 2: In situ activation of pelvic floor and urethral striated muscle progenitor cells. Neurourol Urodyn 38(8):2140–2150. [PubMed: 31452249]

9. Wang B, Ruan Y, Zhou T, et al. 2019. The effects of microenergy acoustic pulses on an animal model of obesity-associated stress urinary incontinence. Part 1: Functional and histologic studies. Neurourol Urodyn 38(8):2130–2139. [PubMed: 31483063]

10. Peng D, Yuan H, Liu T, et al. 2019. Smooth Muscle Differentiation of Penile Stem/Progenitor Cells Induced by Microenergy Acoustic Pulses In Vitro. J Sex Med 16(12):1874–1884. [PubMed: 31585805]

11. Zhang H, Liu M, Kim HT, et al. 2020. Preconditioning improves muscle regeneration after ischemia-reperfusion injury. J Orthop Res. [Epub ahead of print].

12. Ruan Y, Zhou J, Kang N, et al. 2018. The effect of low-intensity extracorporeal shockwave therapy in an obesity-associated erectile dysfunction rat model. BJU Int 122(1):133–142. [PubMed: 29573106]

13. Peng D, Yuan H, Liu T, et al. 2019. Smooth Muscle Differentiation of Penile Stem/Progenitor Cells Induced by Microenergy Acoustic Pulses In Vitro. J Sex Med 16(12):1874–1884. [PubMed: 31585805]

14. Lee C, Agha O, Liu M, et al. 2020. Rotator Cuff Fibro-Adipogenic Progenitors Demonstrate Highest Concentration, Proliferative Capacity, and Adipogenic Potential Across Muscle Groups. J Orthop Res 38(5):1113–1121. [PubMed: 31799698]

15. Justus CR, Leffler N, Ruiz-Echevarria M, et al. 2014. In vitro cell migration and invasion assays. J Vis Exp (88):51046.

16. Jonkman JE, Cathcart JA, Xu F, et al. 2014. An introduction to the wound healing assay using live-cell microscopy. Cell Adh Migr 8(5):440–51. [PubMed: 25482647]

17. Agha O, Mueller-Immergluck A, Liu M, et al. 2020. Intervertebral disc herniation effects on multifidus muscle composition and resident stem cell populations. JOR Spine 3(2): e1091. [PubMed: 32613166]

18. Liao CD, Xie GM, Tsauo JY, et al. 2018. Efficacy of extracorporeal shock wave therapy for knee tendinopathies and other soft tissue disorders: a meta-analysis of randomized controlled trials. BMC Musculoskelet Disord 19(1):278. [PubMed: 30068324]

19. Stania M, Juras G, Chmielewska D, et al. 2019. Extracorporeal Shock Wave Therapy for Achilles Tendinopathy. Biomed Res Int 2019: 3086910. [PubMed: 31950037]

20. Hsiao CC, Huang WH, Cheng KH, et al. 2019. Low-Energy Extracorporeal Shock Wave Therapy Ameliorates Kidney Function in Diabetic Nephropathy. Oxid Med Cell Longev 2019: 8259645. [PubMed: 31354913]

21. Zou ZJ, Liang JY, Liu ZH, et al. 2018. Low-intensity extracorporeal shock wave therapy for erectile dysfunction after radical prostatectomy: a review of preclinical studies. Int J Impot Res 30(1):1–7. [PubMed: 29180799]

22. Myojo M, Ando J, Uehara M, et al. 2017. Feasibility of Extracorporeal Shock Wave Myocardial Revascularization Therapy for Post-Acute Myocardial Infarction Patients and Refractory Angina Pectoris Patients. Int Heart J 58(2):185–190. [PubMed: 28320996]

23. Sun K, Zhou H, Jiang W. 2020. Extracorporeal shock wave therapy versus other therapeutic methods for chronic plantar fasciitis. Foot Ankle Surg 26(1):33–38. [PubMed: 30502222]

24. Mansur NSB, Baumfeld T, Villalon F, et al. 2019. Shockwave Therapy Associated With Eccentric Strengthening for Achilles Insertional Tendinopathy: A Prospective Study. Foot Ankle Spec 12(6):540–545. [PubMed: 30712379]

25. Pavone V, Cannavò L, Di Stefano A, et al. 2016. Low-energy extracorporeal shock-wave therapy in the treatment of chronic insertional achilles tendinopathy: a case series. BioMed Research International 2016:4.

26. Cui K, Kang N, Banie L, et al. 2019. Microenergy acoustic pulses induced myogenesis of urethral striated muscle stem/progenitor cells. Transl Androl Urol 8(5):489–500. [PubMed: 32133280]

27. Hardy D, Besnard A, Latil M, et al. 2016. Comparative Study of Injury Models for Studying Muscle Regeneration in Mice. PLoS One 11(1): e0147198. [PubMed: 26807982]

28. Relaix F, Zammit PS. 2012. Satellite cells are essential for skeletal muscle regeneration: the cell on the edge returns centre stage. Development 139(16):2845–56. [PubMed: 22833472]
29. Almada AE, Wagers AJ. 2016. Molecular circuitry of stem cell fate in skeletal muscle regeneration, ageing and disease. Nat Rev Mol Cell Biol 17(5):267–79. [PubMed: 26956195]
30. Meyer GA. 2018. Evidence of induced muscle regeneration persists for years in the mouse. Muscle Nerve 58(6):858–862. [PubMed: 30159908]
31. Mahdy MA, Lei HY, Wakamatsu J, et al. 2015. Comparative study of muscle regeneration following cardiotoxin and glycerol injury. Ann Anat 202:18–27. [PubMed: 26340019]
32. Wang CJ, Yang YJ, Huang CC. 2011. The effects of shockwave on systemic concentrations of nitric oxide level, angiogenesis and osteogenesis factors in hip necrosis. Rheumatology International 31(7):871–7. [PubMed: 20232068]
33. Yang JP, Lee YN, Son JW, et al. 2019. The Impact of Extracorporeal Shock Wave Therapy on Microcirculation in Diabetic Feet: A Pilot Study. Adv Skin Wound Care 32(12):563–567. [PubMed: 31764146]
34. Christov C, Chrétien F, Abou-Khalil R, et al. 2007. Muscle satellite cells and endothelial cells: close neighbors and privileged partners. Mol Biol Cell 18:1397–1409. [PubMed: 17287398]
35. Kota J, Handy CR, Haidet AM, et al. 2009. Follistatin gene delivery enhances muscle growth and strength in nonhuman primates. Sci Transl Med 1(6):6ra15.
36. Krneta J, Kroll J, Alves F, et al. 2006. Dissociation of angiogenesis and tumorigenesis in follistatin- and activin-expressing tumors. Cancer Res 66(11):5686–95. [PubMed: 16740706]
37. Uezumi A, Ito T, Morikawa D, et al. 2011. Fibrosis and adipogenesis originate from a common mesenchymal progenitor in skeletal muscle. J Cell Sci 124 (Pt24):3654–3664. [PubMed: 22045730]
38. Mozzetta C, Consalvi S, Saccone V, et al. 2013. Fibroadipogenic progenitors mediate the ability of HDAC inhibitors to promote regeneration in dystrophic muscles of young, but not old Mdx mice. EMBO Mol Med 5(4):626–39. [PubMed: 23505062]
39. Fiore D, Judson RN, Low M, et al. 2016. Pharmacological blockage of fibro/adipogenic progenitor expansion and suppression of regenerative fibrogenesis is associated with impaired skeletal muscle regeneration. Stem Cell Res 17(1):161–9. [PubMed: 27376715]
40. Lee C, Liu M, Agha O, et al. 2020. Beige fibro-adipogenic progenitor transplantation reduces muscle degeneration and improves function in a mouse model of delayed repair of rotator cuff tears. J Shoulder Elbow Surg 29(4):719–727. [PubMed: 31784382]
41. Villarroya F, Cereijo R, Villarroya J, et al. 2017. Brown adipose tissue as a secretory organ. Nat Rev Endocrinol 13(1):26–35. [PubMed: 27616452]
42. Wang Z, Liu X, Jiang K, et al. 2020. Intramuscular Brown Fat Activation Decreases Muscle Atrophy and Fatty Infiltration and Improves Gait After Delayed Rotator Cuff Repair in Mice. Am J Sports Med 48(7):1590–1600. [PubMed: 32282238]
43. Lee C, Liu M, Agha O, et al. 2020. Beige FAPs Transplantation Improves Muscle Quality and Shoulder Function After Massive Rotator Cuff Tears. J Orthop Res 38(5):1159–1166. [PubMed: 31808573]
44. Liu M, Wang Z, Lee C, et al. 2020. Brown/Beige Fat Activation after Skeletal Muscle Ischemia-Reperfusion Injury. Muscles Ligaments Tendons J 10 (4):579–588.

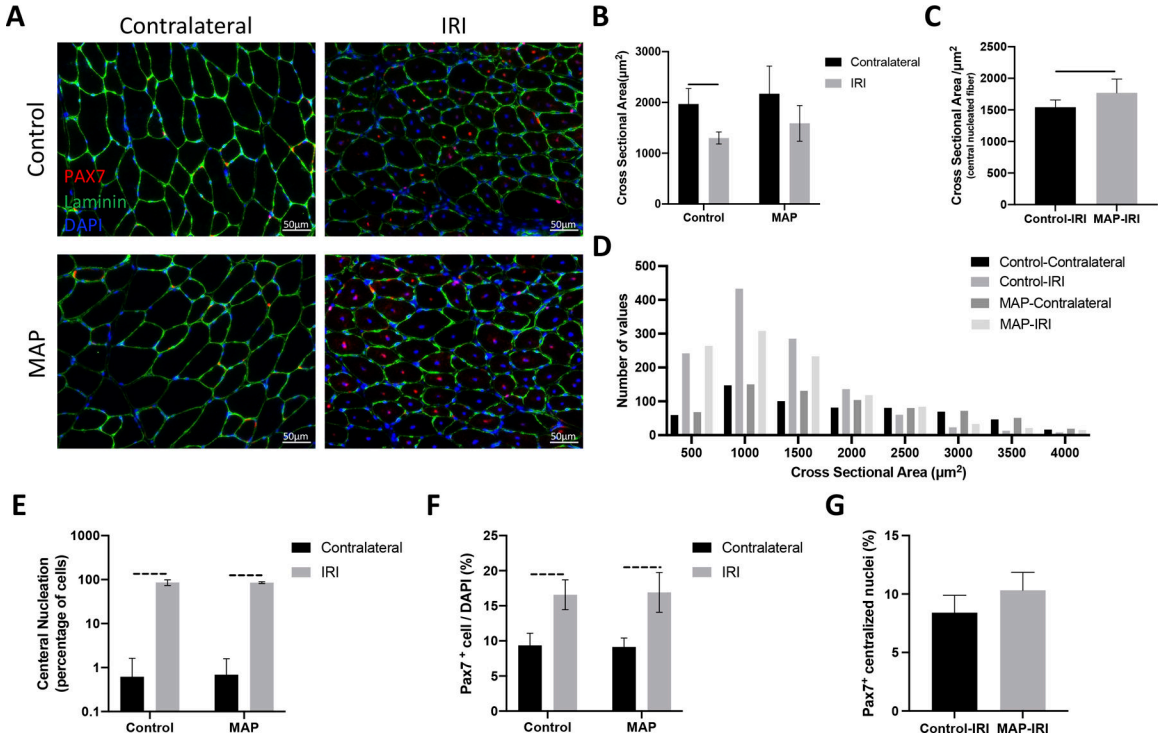

Figure 1.

(A) Representative images of immunofluorescence for Pax7 and laminin. Satellite cells were stained as Pax7 in red and fiber membrane was stained as laminin in green. DAPI represented nuclear in blue. Scale bar: 50μm. (B) No significant change of average CSA was observed in muscles from IRI side between Control and MAP group (n=6 in each group), but the CSA of centrally nucleated fibers in injured muscles significantly increased after MAP treatment 3 weeks post injury (C). (D) Distribution of myofibers sizes in each group. (E) MAP had no effect on muscle central nucleation between Control-IRI and MAP-IRI sides (n=6 in each group). (F) No significant change was found in total Pax7(+) cell / DAPI percentage from Control-IRI and MAP-IRI group. (G) MAP showed a trend in increasing the Pax7(+) centralized nuclei percentage only comparing muslces from Control-IRI and MAP-IRI sides (n=6 in each group). Solid lines indicate $P<0.05$ and dashed lines indicate $P<0.01$.

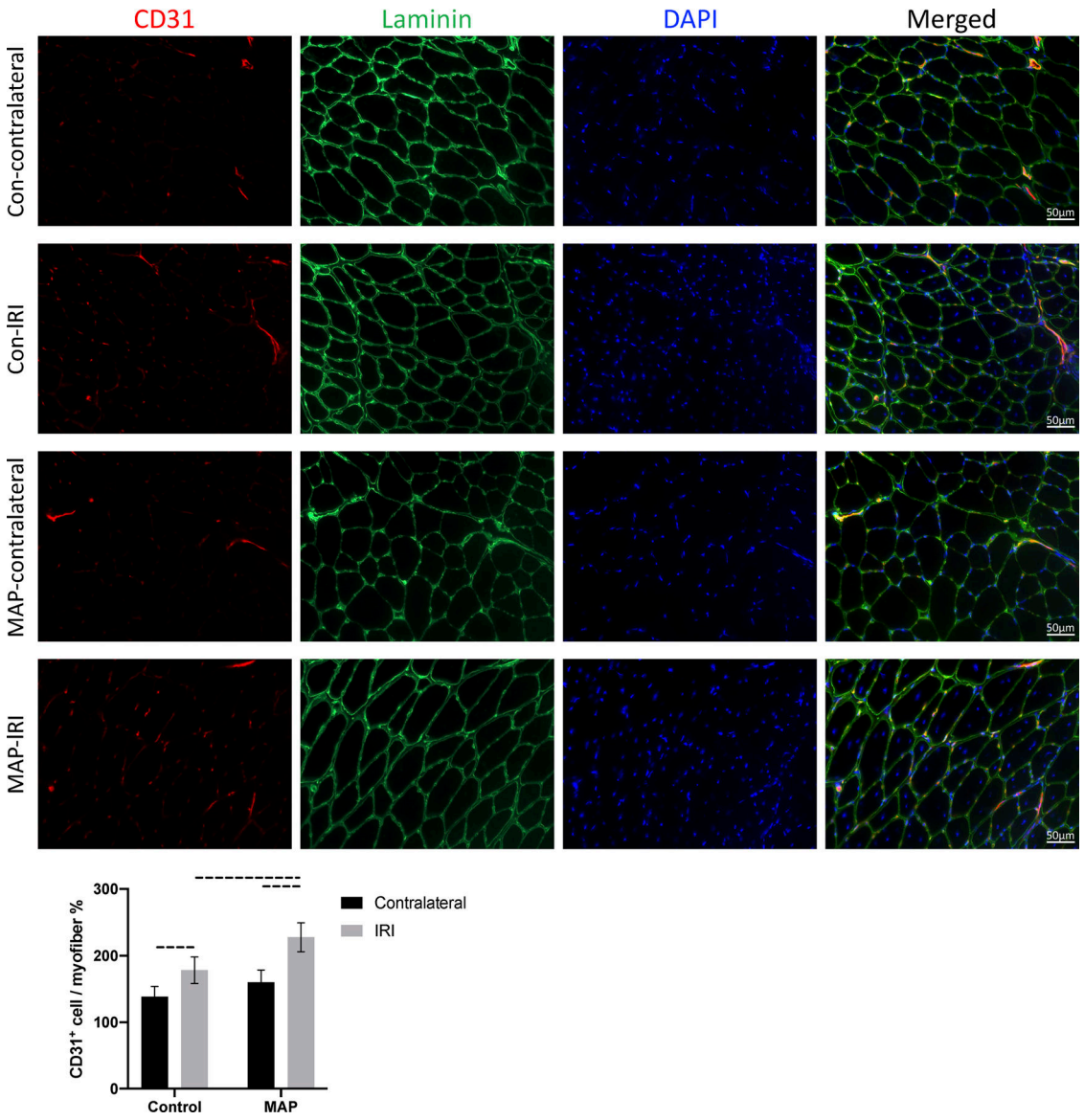

Figure 2.

Representative images of immunofluorescence for CD31 and laminin. Vessels were stained as CD31 in red and fiber membrane was stained as laminin in green. DAPI represented nuclear in blue. Scale bar: 50μm. IR injury induced a significant increase in $CD31^+$ endothelial cell density between Contralateral side and IRI side in both groups, and MAP significantly increased the density in TA muscles from IRI side between Control and MAP groups at 3-week time point after IRI (n=6 in each group). Dashed lines indicate $P<0.01$.

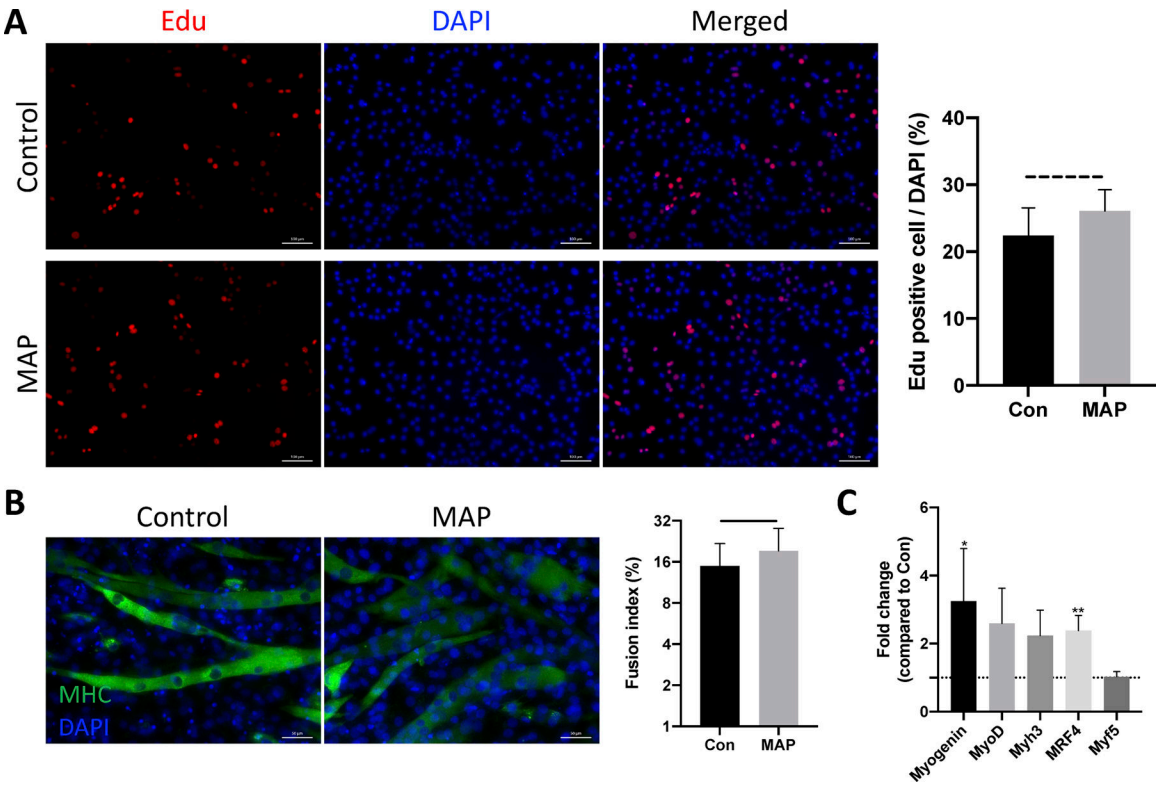

Figure 3.

(A) Representative immunofluorescence images of Edu staining. EdU showed the newly synthesized DNA that stained in red. MAP significantly induced the Edu positive cells in myoblast (n=6 wells in each group). Scale bar: 100μm. (B) Representative immunofluorescence images of MHC staining (n=6 wells in each group). The fusion index significantly increased after 1-week MAP treatment compared to control group. Scale bar: 50μm. (C) mRNA expressions for indicated genes were assessed by quantitative RT-PCR and normalized with 18s rRNA. Results are expressed as mean of fold change compared to control condition. Solid line indicates $P<0.05$ and dashed line indicates $P<0.01$.

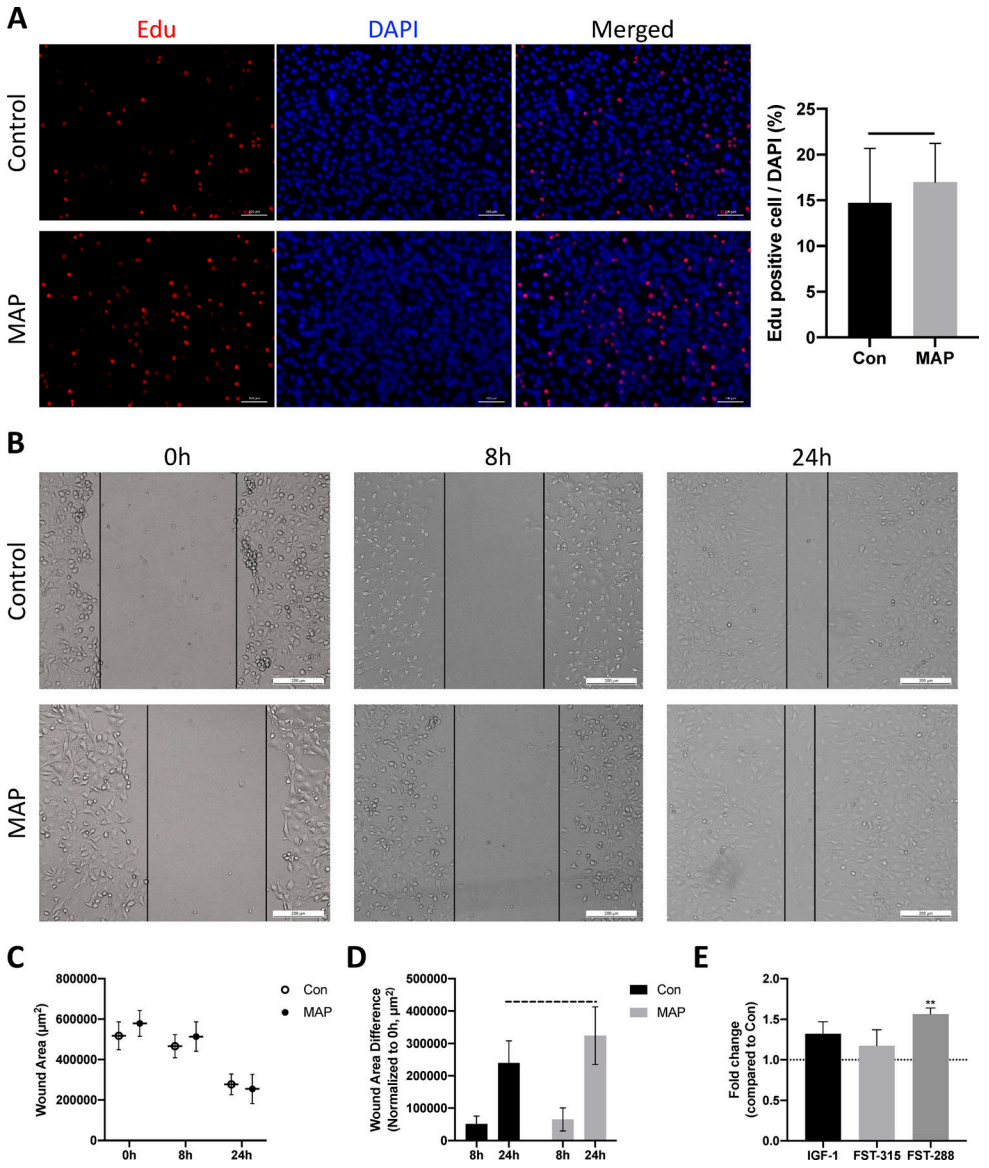

Figure 4.

(A) Representative immunofluorescence images of Edu staining. MAP significantly induced the Edu positive cells / DAPI percentage in endothelial cells compared to control group (n=6 wells in each group). Scale bar: 100μm. (B) Representative images of migration assay taken at 0hr, 8hr and 24hr. MAP accelerated the migration velocity of endothelial cells compared to control cells. Scale bar: 200μm. (C) Wound area at 0hr, 8hr and 24hr in each group and no significant change was found. (D) Wound area difference at 24hr (normalized to 0hr) significantly increased in MAP-treated cells compared to control cells. (E) mRNA expressions for indicated genes were assessed by quantitative RT-PCR and normalized with 18s rRNA. Results are expressed as mean of fold change compared to control condition. Solid line indicates $P<0.05$ and dashed line indicates $P<0.01$.

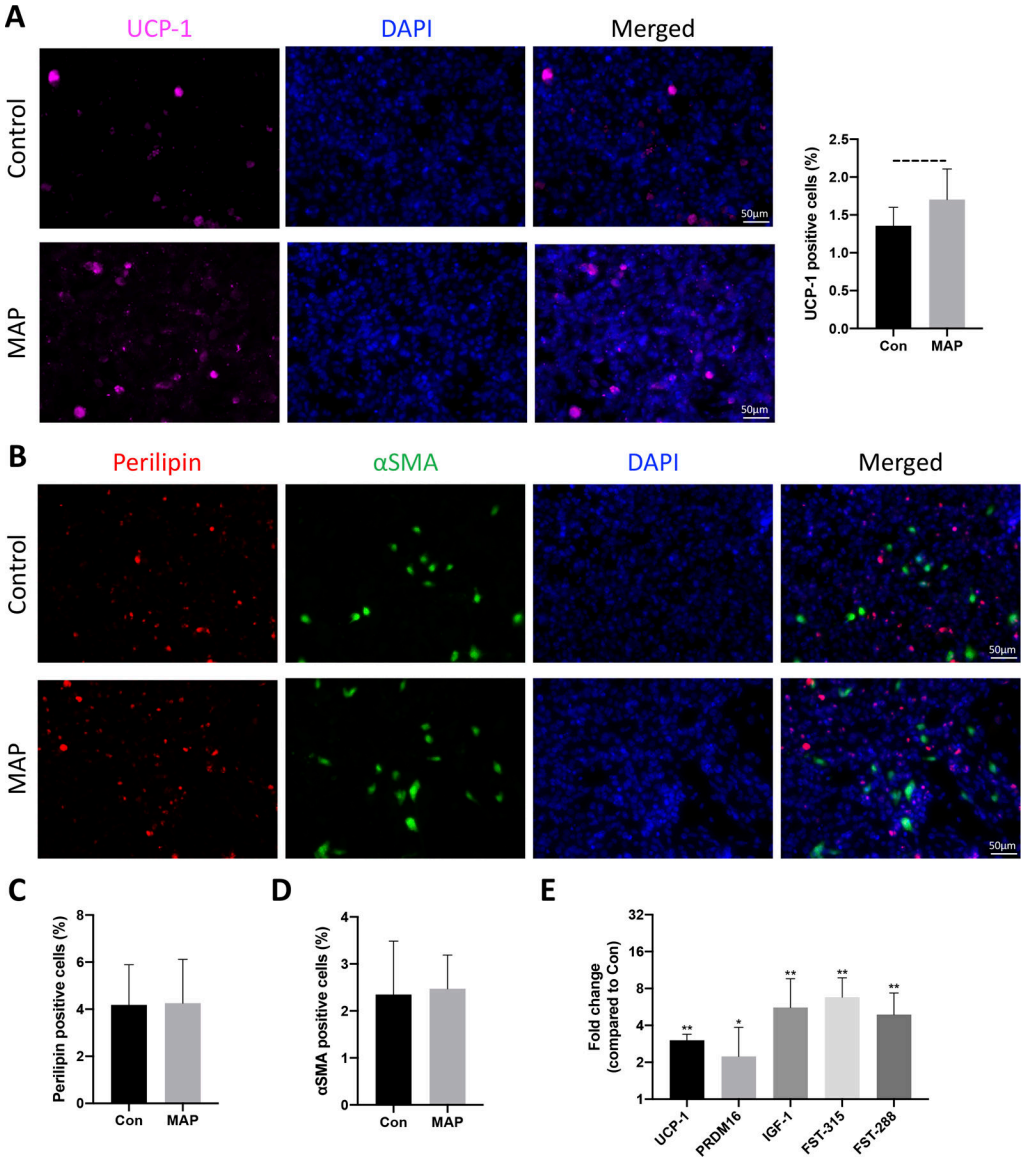

Figure 5.

(A) Representative immunofluorescence images of UCP-1 staining. MAP significantly increased the UCP-1 positive cells / DAPI percentage (n=5 wells in each group). Scale bar: 50μm. (B) Representative immunofluorescence images of Perilipin and α-SMA staining. MAP had no effect on Perilipin (C) and α-SMA (D) positive cells / DAPI percentage compared to cells in control group (n=5 wells in each group). Scale bar: 50μm. (E) RT-PCR showed that mRNA expression levels for UCP-1, PRDM-16, IGF-1, FST-315 and −288 were significantly increased in FAPs after MAP treatment compared to control cells. Results are expressed as mean of fold change compared to control condition. Scale bar: 50μm. Dashed line indicates $P<0.01$.

Table 1

Primer Sequences

Gene	Forward	Reverse
Myogenin	TCCCAACCCAGGAGATCATT	TCAGTTGGGCATGGTTTCGT
MyoD	CCCCGGCGGCAGAATGGCTAC	GGTCTGGGTTCCCTGTTCTGTGT
Myh3	ATGAGTAGCGACACCGAGATG	ACAAAGCAGTAGGTTTTGGCAT
MRF4	ATTCTTGAGGGTGCGGATTTCCTG	AAGACTGCTGGAGGCTGAGGCATC
Myf5	GAGCTGCTGAGGGAACAGGTGGAGA	GTTCTTTCGGGACCAGACAGGGCTG
IGF-1	CAGGCTATGGCTCCAGCAT	GGAAGCAACACTCATCCACA
Follostatin-315	CTCTCTCTGCGATGAGCTGTGT	TCTTCCTCCTCCTCCTCTTCCT
Follostatin-288	CTCTCTCTGCGATGAGCTGTGT	GGCTCAGGTTTTACAGGCAGAT
UCP-1	AGGCTTCCAGTACCATTAGGT	CTGAGTGAGGCAAAGCTGATTT
PRDM16	TATGGAGCTAGGCAGGGACA	TCCATACATCAGGGAGCAGA
18s	CTCTGTTCCGCCTAGTCCTG	AATGAGCCATTCGCAGTTTC